# NUMERICAL STUDY OF A ROTARY KILN. CASE OF AN INDUSTRIAL PLANT IN PARAGUAY

**Hugo Gonzalez, hgonzalez@ing.una.py**[1]
**Cristhian Zarate, czarate@ing.una.py**[1]
**Dario Alviso, dalviso@ing.una.py**[1,2]
**Juan Carlos Rolon, jcrolon@ing.una.py**[1]
[1]Laboratorio de Mecánica y Energía, Facultad de Ingeniería, Universidad Nacional de Asunción, Campus Universitario, San Lorenzo, 2160 Paraguay
[2]Laboratorio de Fluidodinámica, Facultad de Ingeniería, Universidad de Buenos Aires, Paseo Colón 850 CABA Argentina

***Abstract:*** *This paper summarizes the results obtained from the modeling and simulation of an industrial rotary kiln used for clinker production in order to optimize its operation and reduce fuel consumption. The model includes a sub-model for the variation of bed height within the kiln and another for simulating key processes occurring in solid bed taking into account the chemical reactions taking place during clinker formation and heat transfer in rotary kilns. Chemical reactions were considered as ad hoc models. Melt formation near burner zone was also taken into account. The gas and shell temperature profiles of the kiln were specified. The energy conservation equation was solved using a differential equation solver available in Matlab®. The model was used to simulate the performance of an industrial rotary kiln in Paraguay and investigate the influence of operating parameters on energy consumption of the kiln in order to minimize it.*
***Keywords:*** *Rotary kilns, Portland Cement, Industrial Plant*

## 1. NOMENCLATURE

$A_{cl}$: Cross-sectional area covered by the clinker.
$A_{CGW}$: Convection area from gas to wall.
$A_{CGB}$: Convection area from gas to bed.
$A_{CWB}$: Conduction area from wall to bed.
$A_{RGB}$: Radiation area from gas to bed.
$A_{RWB}$: Radiation area from wall to bed.
$C_C$: Mass concentration of $CaCO_3$ particle.
$C_k$: Mass concentration of *k*th reactant.
$C_p$: Specific heat of the bed.
$C_{p,CO_2}$: Specific heat of $CO_2$.
$C_T$: Coating thickness.
$C_{T,max}$: Maximum coating thickness.
$D$: Inner diameter of the kiln.
$D_e$: Hydraulic diameter.
$E_{aj}$: Activation energy of the *j*th reaction.
$h_{cl}$: Height of solid bed.
$h_{CGB}$: Coefficient for convection from gas to bed.
$h_{CGW}$: Coefficient for convection from wall to bed.
$h_{CWB}$: Coefficient for conduction wall and bed.
$H$: Heat of reaction.
$k_B$: Bed thermal conductivity.
$k_G$: Gas thermal conductivity.
$k_{app}$: Rate constant for shrinking core model.
$k_{s0}$: Arrhenius factor for calcination.
$k_{0j}$: Arrhenius factor for *j*th reaction.
$L$: Kiln length.
$L_{gcl}$: Cord of the sector covered by clinker.
$\dot{m}$: Mass flow rate.
$m_L$: Fraction of liquid formed due to melting.
$M_W$: Molecular weight.
$M_j$: Stoichiometric coefficient of the base component.
$n$: Kiln rotational speed, rpm.
$NC$: Number of base compounds at *j*th reaction.
$NR$: Number of reactions.
$Q$: Heat gained by the bed due to heat transfer.
$Q_{CGW}$: Convection from gas to wall.
$Q_{CGB}$: Convection from gas to bed.
$Q_{CWB}$: Conduction from wall to bed.
$Q_{COAT}$: Heat transfer through coating.
$Q_{CO_2}$: Heat loss due to $CO_2$ migration.
$Q_{LOSS}$: Heat loss to the environment.
$Q_{RGB}$: Radiation from gas to bed.
$Q_{COAT}$: Heat transfer through refractory bricks.
$Q_{RWB}$: Radiation from wall to bed.
$Q_{STL}$: Heat transfer through steel shell.
$R$: Inner radius of the kiln.
$R_0$: Initial $CaCO_3$ particle radius.
$R_i$: Rate of reaction.
$R_{CO_2}$: Rate of formation of $CO_2$.
$Re_D$: Axial Reynolds number.
$Re_\omega$: Angular Reynolds number.
$T_B$: Temperature of the bed.
$T_G$: Temperature of the gas.
$T_L$: Liquidus temperature.
$T_S$: Solidus temperature.
$T_W$: Temperature of the inner wall.
$T_{coat}$: Temperature for $C_{T,max}$ to be reached.
$u_g$: Axial velocity of gas.
$v_{cl}$: Axial velocity of solid bed.
$Y_i$: mass fraction of the *i*th species in the bed.
$z$: axial distance in the kiln.
$Z_{ij}$: Stoichiometric coefficients.

***Greek letters***.

$\beta$: Angle of repose of solids.
$\theta$: Kiln inclination.
$\rho$: Bulk density of the bed.
$\varepsilon$: Half of the angle made by solids at the center of kiln.
$\lambda$: Latent heat of melting
$\alpha_G$: Gas absorptivity.
$\omega$: Kiln rotational speed, rad/s.
$\epsilon_B$: Bed emissivity.
$\epsilon_G$: Gas emissivity.
$\epsilon_W$: Inner wall emissivity.
$\epsilon_s$: Solid porosity.
$\mu_g$: Gas viscosity.
$\Omega$: Form factor for radiation.

## 2. INTRODUCTION

Rotary kilns are large units, (40 to 70 m in length and 1.5 to 5 m in diameter) slightly tilted to the horizontal (between $1^\circ$ to $3^\circ$) and rotating on its axis (2 to 6 rpm) in order to ease the transport of material. Additionally, they are coated with a refractory material on the inside. They are basically heat exchangers in which the thermal energy of a hot gas flowing counter-currently is transferred to the solids bed. Rotary kilns are employed by industry to carry out a wide variety of material processing, for example calcination of limestone, reduction of oxide ore, reclamation of hydrated lime, calcining of petroleum coke, etc. (Boateng & Barr, 1996), but its main usage is in the cement industry, where is used to convert calcineous raw meal to cement clinker. A schematic representation of clinker production is shown in Fig. 1. Raw meal for cement production is a mixture of predetermined proportions of limestone, silica and small quantities of iron and alumina oxide (Darabi, 2007). The raw meal is first fed to pre-calciners where about 60 – 80% of calcination takes place. Then, the partially calcined material is fed to the rotary kiln. The main function of rotary kilns is to provide a high temperature environment in order to drive the chemical reactions for clinker formation (Mujumdar & Ranade, 2006a), which is an endothermic process. The energy required to carry out these reactions is provided by the burning of a fuel, in Paraguay usually fuel oil and pet coke.

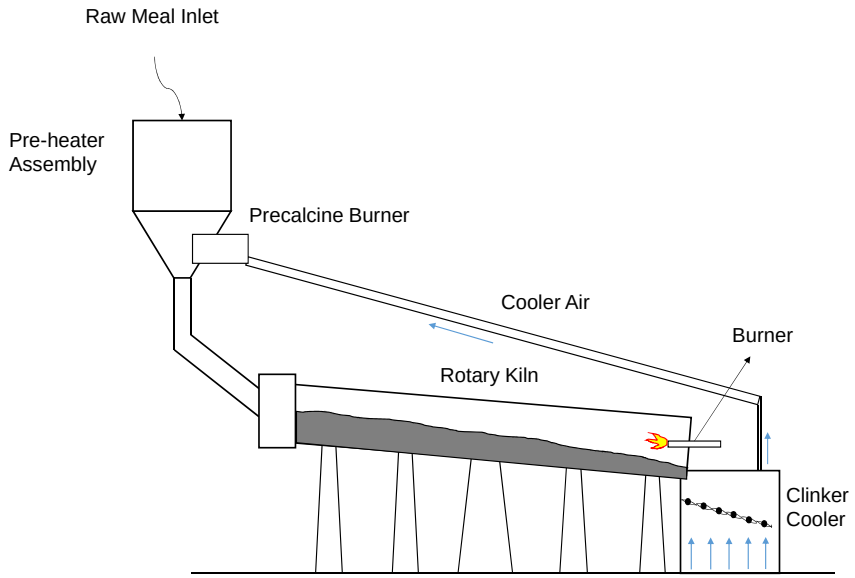


Figura 1: **Schematic representation of clinker production.**

The cement industry is a major consumer of energy, with a typical specific energy use of about 3.2 MJ/kg of clinker manufactured. This is because the reaction $\mathrm{CaCO_3} \rightarrow \mathrm{CaO} + \mathrm{CO_2}$, the first step of clinker formation, is highly endothermic (Mastorakos *et al*., 1999). Clinker formation takes place at a temperature between 1200 to $1500^\circ$C. In the initial part of the kiln, the raw meal is calcined. Then, the solids undergo solid-solid reactions as they move forward. The final reaction takes place in liquid phase. Melt formation also helps nodulization to produce cement clinker. Clinker is then transferred to a clinker cooler to recover energy (Mujumdar & Ranade, 2006a).

The simulation of rotary kilns is of special interest since its operating conditions hinder the development of experimental studies. The performance of a rotary kiln controls the cement quality and the overall plant performance. According to Mujumdar and Ranade (2006a), despite of being a key equipment, attempts of developing computational models to simulate cement kiln operation are few. In the past years, computational fluid dynamics (CFD) based models are being applied to simulate rotary kilns (Mastorakos *et al*., 1999; Ranade, 2003). With these models it is possible to simulate quite accurately the burner and gas region of a rotary kiln. It is however difficult to model motion of solid particles in a conventional CFD framework. In the other hand, using a one-dimensional model for the reactions taking place in the solid bed can give reasonable results, but its usage for modelling the gas region can be inaccurate. It is possible then to use a separate one-dimensional model for the solid bed, and either experimental data or a three-dimensional CFD model for the gas region.

In this paper we present a one-dimensional model for simulating the rotary cement kiln of a Paraguayan plant. The one-dimensional model developed by Mujumdar and Ranade (2006a), is used along with experimental data obtained for gas phase. The model accounts for variation of bed height as a function of kiln operating conditions and solid properties and also for melt formation during material passage along high temperature zones. The model was used to simulate the performance of the rotary kiln and the numerical results were analyzed.

## 3. MODELING OF ROTARY KILNS.

There are very important issues that must be considered when developing a mathematical model of a rotary kiln, such as axial motion of solids inside the kiln, heat transfer between the gas region, solids and inner wall, chemical reactions in the bed, reduction of the solids mass flow rate, phase transition of the material from solid to liquid during its passage along the kiln and coating formation. Each of these issues are discussed in the following.

A partially calcined raw meal is fed to the top of the kiln with a certain flow rate and due to the rotation and tilt, it moves from the upper to the bottom of the kiln. Axial motion of solids is dependent on operational parameters such as mass flux, speed of rotation, angle of repose of the material and kiln tilt (Mujumdar & Ranade, 2006a). During the passage of the material through the kiln, the area occupied by the solids and the axial velocity change as the height varies. These phenomena affect the residence time of the material inside the kiln, which is important for an accurate simulation of the chemical reactions and heat transfer. In their work, Mujumdar and Ranade, (2006a) explained that several models for predicting the residence time and height variation along the kiln were developed. One of the first reported in the literature was proposed by Sullivan *et al*. (1927). From that model, there have been subsequent studies (Saeman, 1951; Kramers & Croockewit, 1952; Lebas *et al*., 1995, etc.). Obviously, changes in operating parameters have effect on kiln performance, therefore, choosing a model that predicts this influence accurately is crucial.

Heat transfer in rotary kilns is extremely important since it leads the chemical reactions in the bed that will eventually produce clinker; as the solid material flows, it gains heat, and its temperature increases. Hence, heat transfer needs to be modeled accurately. The three fundamental mechanisms of heat transfer are present in these devices. A schematic representation of heat transfer in the transverse section of the kiln is shown in Fig. 2 as presented in Mujumdar and Ranade (2006a). The hot gases transfer energy to the inner wall and bed by radiation and convection while heat transfer between the bed and inner wall is by radiation and conduction. Heat is also transferred through the refractory bricks (when formed, it will flow through coating first) and the steel shell and eventually will be lost to the environment. For operating conditions existing in cement kilns, heat transfer is carried out mainly by radiation (Mujumdar & Ranade, 2006a).

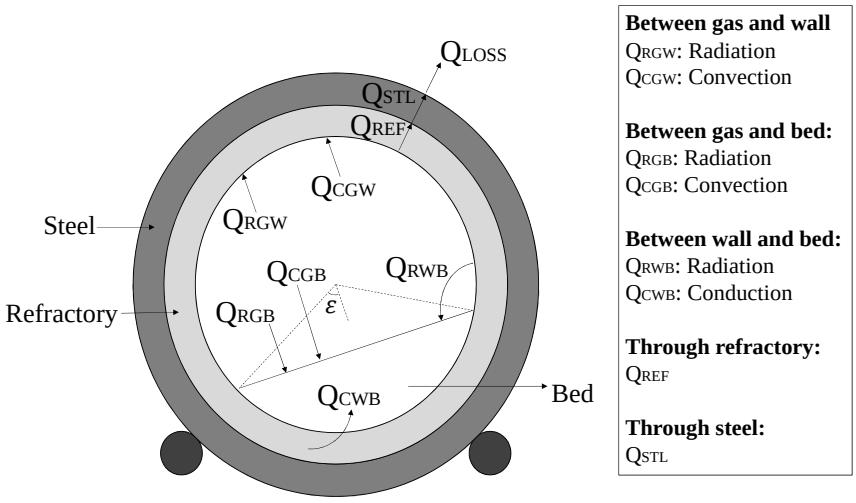


Figura 2: **Heat transfer in a rotary kiln.**

Divers chemical reactions occurs in the bed along the kiln. These can be solid-solid or solid-liquid reactions (Mujumdar & Ranade, 2006a). Raw materials for clinker manufacturing are limestone and clay, being the main compounds $CaCO_3, SiO_2, Al_2O_3$ and $Fe_2O_3$. The raw meal is first passed through a set of pre-calciner cyclones where it reaches calcination temperature and is partially calcined. The $CaCO_3$ is decomposed into $CaO$ and $CO_2$, so the material composition at kiln inlet consists of the first four compounds and $CaO$. In their work, Mujumdar and Ranade, (2006a) explained that some authors have reported formation of several species within the kiln, however, some of them are present in insignificant amounts and are neglected for modeling purposes. The most important species considered in clinker composition after chemical reactions are tricalcium silicate (alite), dicalcium silicate (belite), tricalcium aluminate and tetracalcium aluminoferrite, being denoted by a special notation used by cement chemist as C3S, C2S, C3A and C4AF respectively (Mastorakos *et al*., 1999) . The five major reactions considered by most of the researchers are given in Tab. 1. In the initial part of the kiln the remaining calcination occurs (Reaction 1). During this reaction, the $CO_2$ content of the bed is released and transferred to the hot gas. Because of this, the solid mass flow rate will gradually decrease. Reaction 3, considered to be the final step in clinker formation, occurs at high temperatures and only at presence of liquid phase (Mastorakos *et al*., 1999). When simulating rotary kilns, is very important, as in any chemical reactor, to have kinetics information that

allows to represent the reactive process adequately. Calcination reaction has been studied extensively. Several models have proposed to study decomposition of calcium carbonate. It was shown that limestone calcination is a shrinking core process (Mujumdar & Ranade, 2006a). This reaction is the only one that has available kinetics parameters obtained by theoretical and experimental analysis. However, there are scarce or none studies about the other reactions. In the present work, the shrinking core model has been used for the calcination reaction and simple Arrhenius type expressions for the other reactions.

Tabela 1: **Chemical reactions and heat of reactions.**

| | Reaction | | ΔH (J/mol) |
|---|---|---|---|
| 1. | $CaCO_3 \rightarrow CaO + CO_2$ | | 178350 |
| 2. | $2CaO + SiO_2 \rightarrow C2S$ | $C2S = 2CaO \cdot SiO_2$ | -126420 |
| 3. | $C2S + CaO \rightarrow C3S$ | $C3S = 3CaO \cdot SiO_2$ | 85590 |
| 4. | $3CaO + Al_2O_3 \rightarrow C3A$ | $C3A = 3CaO \cdot Al_2O_3$ | 21800 |
| 5. | $4CaO + Al_2O_3 + Fe_2O_3 \rightarrow C4AF$ | $C4AF = 4CaO \cdot Al_2O_3 \cdot Fe_2O_3$ | -41300 |

Another important issue to take into account, is the formation of melt along the kiln. When the temperature reaches a certain value, the solid material begin to form the liquid phase, which is essential for C3S formation. The amount of melt formed will depend on the temperature profile of the bed. As the melt phase is formed, it forms coating over the refractories in the last meters of the kiln. The formation of the coating is beneficial for the refractory life (Mujumdar & Ranade, 2006a) and also helps to reduce the temperature of the kiln shell since heat from the inside now flows through coating first. Mathematical equations used to model all the aspects discussed before are explained next.

## 4. MATHEMATICAL EQUATIONS

### 4.1 Solids motion along the kiln.

To predict the bed height variation of the solids along the kiln, the Saeman's model was used. Equation (1) represents the Saeman's equation to the model.

$$\frac{dh}{dz} = \frac{3\tan(\beta)}{4\pi n}\frac{\dot{m}}{\rho}[R^2 - (h-R)^2]^{-3/2} - \frac{\tan(\theta)}{\cos(\beta)} \tag{1}$$

As seen in Figure 2, *h* is related to the fill angle $\varepsilon$, and Equation (1) can be rewritten as follow (Danish *et al*, 2012):

$$\frac{d\varepsilon}{dz} = \frac{3\tan(\beta)}{4\pi n R^4}\frac{\dot{m}}{\rho}\frac{1}{\sin^4(\varepsilon)} - \frac{\tan(\theta)}{R\cos(\beta)}\frac{1}{sin(\varepsilon)} \tag{2}$$

An exact analytical solution developed by Danish *et al* (2012) was used to solve Equation (2). Then, the variation of bed height, variation of the area occupied by the solids and axial velocity profile were calculated as (Ngako *et al*, 2015):

$$h_{cl} = R[1-\cos(\varepsilon)] \quad ; \quad A_{cl} = R^2[\varepsilon - \frac{1}{2}\sin(2\varepsilon)] \quad ; \quad v_{cl} = \frac{\dot{m}}{\rho A_{cl}} \tag{3}$$

### 4.2 Heat transfer

#### 4.2.1 Radiation.

Heat transfer by radiation is the main mechanism transfer. Radiation occurs between: gas phase and bed, gas phase and kiln internal walls, and kiln internal walls and bed. The first two cases were evaluated by the equations developed by Hottel and Sarofim (1967) as shown in the work of Mujumdar and Ranade (2006a) :

$$Q_{RGK} = \sigma A_{RGK}(\epsilon_K + 1)\Big(\frac{\epsilon_G T_G^4 - \alpha_G T_K^4}{2}\Big) \qquad K = B, W \tag{4}$$

Subscript *B* denotes solid bed and *W* denotes walls.

Heat transfer between exposed internal walls and bed is given by:

$$Q_{RWB} = \sigma \times A_{RWB} \times \epsilon_B \times \epsilon_W \times \Omega \times (T_W^4 - T_B^4) \quad ; \quad \Omega = \frac{L_{gcl}}{(2\pi - 2\varepsilon)R} \tag{5}$$

Where $\Omega$ represents the form factor of radiation.

#### 4.2.2 Convection.

Convective heat transfer between gas phase and bed, and gas phase and kiln internal walls was evaluated as (Mujumdar & Ranade, 2006a):

$$Q_{CGK} = h_{CGK} A_{CGK} (T_G - T_K) \tag{6}$$

The heat transfer coefficients for convection were calculated using Tscheng and Watkinson's work (1979):

$$h_{CGB} = 0.46 \frac{k_G}{D_e} Re_D^{0.535} Re_\omega^{0.104} \eta^{-0.341} \quad ; \quad h_{CGW} = 1.54 \frac{k_G}{D_e} Re_D^{0.575} Re_\omega^{-0.292} \tag{7}$$

The axial and angular Reynolds numbers were calculated as (Mujumdar & Ranade, 2006a):

$$Re_D = \frac{\rho_g \times u_g \times D_e}{\mu_g} \quad ; \quad Re_\omega = \frac{\rho_g \times \omega \times D_e^2}{\mu_g} \tag{8}$$

$$D_e = \frac{R(2\pi - 2\varepsilon + \sin(2\varepsilon))}{\pi - \varepsilon + \sin(\varepsilon)} \tag{9}$$

$$\eta = \frac{2\varepsilon - \sin(2\varepsilon)}{2\pi} \tag{10}$$

And the thermal conductivity of the gas phase was calculated by the expression used in Mujumdar & Ranade (2006a):

$$k_G = -7.494\times10^{-3} + 1.709\times10^{-4} T_G - 2.377\times10^{-7} T_G^2 + 2.202\times10^{-10} T_G^3 - 9.463\times10^{-14} T_G^4 + 1.581\times10^{-17} T_G^5 \tag{11}$$

#### 4.2.3 Conduction.

The heat transfer between the bed and the covered internal walls were calculated as:

$$Q_{CWB} = h_{CWB} A_{CWB} (T_W - T_B) \tag{12}$$

Where $h_{CWB}$ was evaluated using empirical correlation given by Tscheng and Watkinson (1979) as:

$$h_{CWB} = 11.6 \frac{k_B}{A_{CWB}} \left( \frac{2\omega R^2 \varepsilon}{\alpha_B} \right)^{0.3} \tag{13}$$

### 4.3 Chemical reactions and conservation equations.

The rate expression for Reaction 1 was described using a shrinking core model as (Mujumdar & Ranade, 2006a):

$$\frac{dC_c}{dt} = k_{app} C_C^{2/3} e^{(-E_a/RT)} \quad \text{where} \quad k_{app} = \frac{3\varepsilon_s^{1/3} k_{s0}}{R_0} \left( \frac{M_W}{\rho} \right)^{2/3} \tag{14}$$

The rate expression for the rest of the reactions were calculated as (Mujumdar & Ranade, 2006a):

$$R_i = \sum_{j=1}^{NR} \frac{Z_{ij}}{M_j} k_{0j} e^{(E_{aj}/RT_B)} \prod_{k=1}^{NC} C_k \tag{15}$$

Equation (15) assumes that all reactions are of first order with respect to each reactant. It is important to emphasize that these are ad hoc models and the Arrhenius parameters were chosen to match the expected composition at the kiln exit.

Mass conservation for species *i* and overall mass conservation equations were considered respectively as (Mujumdar & Ranade, 2006a):

$$\frac{d(A_{cl} v_{cl} \rho Y_i)}{dz} = R_i A_{cl} \quad ; \quad \frac{d(A_{cl} v_{cl} \rho)}{dz} = -R_{CO_2} A_{cl} \tag{16}$$

Where $R_{CO_2}$ is the rate of formation of $CO_2$.

The energy conservation equation taking into account the variation of bed density and migration of $CO_2$ to gas phase, was written in terms of the bed temperature $T_B$ as (Coral, 2011):

$$\frac{dT_B}{dz} = \frac{QL_{gcl} + \sum_{i=1}^{NR} (\Delta H R_i) - Q_{CO_2}}{A_{cl} \rho v_{cl} C_p} - \left( T_B + \frac{\lambda m_L}{C_p} \right) \left( \frac{1}{\rho} \frac{d\rho}{dz} \right) \tag{17}$$

*Q* is the heat flux received by the bed from the gases and inner wall and it was calculated as (Mujumdar & Ranade, 2006):

$$Q = \frac{Q_{CWB}}{A_{CWB}} + \frac{Q_{RWB}}{A_{RWB}} + \frac{Q_{RGB}}{A_{RGB}} + \frac{Q_{CGB}}{A_{CGB}} \tag{18}$$

$\Delta H$ is the heat of reaction and its temperature dependence was taken into account. The values shown in Table 1 were corrected at each bed temperature along the kiln. $Q_{CO_2}$ is the volumetric energy sink due to $CO_2$ loss from the bed and was calculated as (Mujumdar, 2008):

$$Q_{CO_2} = -R_{CO_2} \times C_{p,CO_2} \times (T_{CO_2,avg} - T_{base}) \tag{19}$$

Where $T_{CO_2,avg}$ is the average temperature of the bed in the calcination region and it was considered as 1000 K. $T_{base}$ = 298 K.

The term $\lambda m_L$ represents the energy required for melting solids where $\lambda$ is the latent heat of melting and it was considered as $\lambda$ = 416 kJ/kg (Mastorakos *et al*., 1999). The modeling of melt phase is explained in the next section.

Finally, heat balance equations were written as (Mujumdar & Ranade, 2006a):

$$Q_{RGW} + Q_{CGW} - Q_{RWB} - Q_{CWB} = Q_{COAT} = Q_{REF} = Q_{STL} = Q_{LOSS} \tag{20}$$

### 4.4 Melting of solids and coating.

Melting of solids in the kiln was assumed to be proportional to the bed temperature in the kiln. Melting was modelled by using the following relationship between mass fraction of liquid and bed temperature (Mujumdar & Ranade, 2006a):

$$m_L = max\Big[0, \frac{T_B - T_S}{T_L - T_S}\Big] \tag{21}$$

$T_L$ represents the temperature at which all mass is liquid and $T_S$ is the temperature at which first drop of liquid forms. According to Mujumdar & Ranade (2006a), the values of $T_L$ and $T_S$ depend on the composition of solids in the kiln and may vary within the kiln. These values were assumed to be constant and were chosen in order to match mass fraction of liquid at certain temperatures according to available data of the industrial kiln in study. It was found that these values were $T_S$=1400 K and $T_L$=2644 K.

Coating formation over kiln inner walls is a complex phenomenon. Its interaction with design and operating parameters are not yet well-understood. In practice, usually coating thickness is measured under cold conditions. Some of the data on maximum coating thickness available from industrial sources and the values reported by Mastorakos *et al.* (1999) indicate that the maximum coating thickness varies within the range of 0.03D < $C_{T,max}$ < 0.05D, (Mujumdar & Ranade, 2008) where D is the internal diameter of the refractories. In this case, there was no information about the maximum coating thickness and it was set to 0.04D. As mentioned earlier, coating starts forming when the bed temperature exceeds $T_S$ and it attains a maximum thickness after some point. In the absence of any better information, in this work, we have assumed that the coating thickness varies linearly with the bed temperature up to a certain limit and then remains constant thereafter. Thus, the coating thickness ($C_T$) along the kiln length was calculated as (Mujumdar & Ranade, 2006b):

$$C_T = \Big(\frac{T_B - T_S}{T_{coat} - T_S}\Big) C_{T,max} \quad \text{for} \quad T_S < T_B < T_{coat} \tag{22}$$

$T_{coat}$ is the temperature at which maximum coating thickness, $C_{T,max}$, is reached and it was set to 1600 K. If $T_B$ < $T_S$ then $C_T = 0$. When $T_B > T_S$, $C_T = C_{T,max}$

## 5. SIMULATION OF THE INDUSTRIAL KILN

To simulate the performance of the rotary kiln, it is necessary to specify the temperature profile of the kiln shell since the temperature profile of the inner walls is unknown. In this case, data was obtained from in-field measurements of the shell temperature and then were used to obtain the inner walls temperature profile using a Newton-Raphson subroutine. The obtained profile was then used to solve the equations showed in section 3.2. It is also necessary to know the gas phase temperature profile along the kiln. In this work we use an approximation of the gas temperature profile, based on the CFD model developed by Ranade (2003), where it is seen that this profile can be fitted as two linear profiles touching each other at maximum temperature. The location of this point in the kiln is referred as maximum flame position and the temperature at this point is referred as maximum flame temperature (Mujumdar & Ranade, 2006a). The maximum flame position was considered to be at 0.7L, where *L* is the length of the kiln. The maximum flame temperature was calculated using the theoric flame temperature formula for fuel-oil (Duda, 1977) and it was set to 2396 K. Gas temperature at burner solid entry and burner end were set as 1325 K and 1375 K respectively.

The mass flow rate, temperature of the solids and mass fractions of the charge at kiln inlet are required to specify the initial conditions to the model. These and other operating parameters of the kiln are shown in Tab. 2. Physical properties used in the model are shown in Tab. 3. The rotary kiln in study uses 4 different types of refractories along the kiln and the thermal conductivity of each type varies with its composition.

As expressed before, chemical reactions were *ad hoc* models. For the first reaction, values for the activation energy and pre-exponential factor were chosen as proposed by Rao *et al*, 1989. For the other reactions, activation energy values were used as proposed by Mastorakos *et al*, 1999 and the pre-exponential factors were chosen by trial, to give the expected composition at the kiln exit. The values are shown in Tab. 4. Energy conservation equation was solved using the ode113 solver of the *ordinary diferential equation solver pack* available in Matlab®.

Tabela 2: **Dimensions and operating conditions of the rotary kiln.**

| | Variable | Value |
|---|---|---|
| 1. | Length, m | 56 |
| 2. | Height of dam at kiln exit,m | 0.225 |
| 3. | Inner diameter, m | 3.95 |
| 4. | Refractory thickness, m | 0.2 |
| 5. | Steel shell thickness, m | 0.03 |
| 6. | Speed of rotation, rpm | 3 |
| 7. | Tilt, % | 4 |
| 8. | Mass flow rate, kg/s | 29.86 |
| 9. | Solids temperature at kiln inlet, K | 1123 |
| 10. | Solids temperature at kiln exit, K | 1673 |
| 11. | Gas temperature at solids entry, K | 1325 |
| 12. | Gas temperature at solids exit, K | 1373 |
| 11. | Maximum flame temperature, K | 2396 |
| 12. | Mass fraction of $CaCO_3$ at kiln inlet | 0.383 |
| 13. | Mass fraction of $CaO$ at kiln inlet | 0.338 |
| 14. | Mass fraction of $SiO_2$ at kiln inlet | 0.178 |
| 15. | Mass fraction of $Al_2O_3$ at kiln inlet | 0.0411 |
| 16. | Mass fraction of $Fe_2O_3$ at kiln inlet | 0.0355 |
| 17. | Mass fraction of melt phase at 1611 K | 0.19 |
| 18. | Mass fraction of melt phase at 1723 K | 0.27 |

Tabela 3: **Physical properties.**

| | Variable | Value |
|---|---|---|
| 1. | Bed density, kg/$\mathrm{m}^3$ | 1380 |
| 2. | Bed heat capacity, kJ/kg K | 0.8[1] |
| 3. | Bed emissivity | 0.9[2] |
| 4. | Bed diffusivity | 0.9 |
| 5. | Wall emissivity | 0.9[2] |
| 6. | Bed thermal conductivity, W/m K | 0.5[3] |
| 7. | Refractories thermal conductivity, W/m K | 1.5 - 2.45 - 2.1 - 4.65[4] |
| 8. | Gas heat capacity | (0.106 $T_G$ + 1173)[5] |
| 9. | Gas viscosity | (0.1672 $\times 10^{-5}$ $\sqrt{T_G}$ - 1.058 $\times 10^{-5}$)[5] |
| 10. | Gas density, kg/$\mathrm{m}^3$ | 0.8[6] |
| 11. | Gas velocity, m/s | 5 |
| 12. | Gas emissivity, K | 0.1[7] |
| 13. | Steel shell thermal conductivity, W/m K | 52[8] |
| 14. | Coating thermal conductivity, W/m K | 0.73[9] |
| 15. | Solid porosity | 0.4[10] |
| 16. | Initial $\mathrm{CaCO_3}$ particle radius, m | $(1 \times 10^{-4})$[10] |

[1]Martin (1932); [2]Mujumdar and Ranade (2006); [3]Perry (1997); [4]Harbison-Walker Handbook (2005)
[5]Guo *et al*.(2003); [6]Spang(1972); [7]Silcox&Perching(1990); [8]http://www.engineersedge.com/properties_of_metals.html
[9]Al-Yasiri *et al*. (2012); [10]Irfan and Doğu (2001).

Tabela 4: **Arrhenius parameters for chemical reactions models.**

| Reaction | Activation Energy* (J/mol) | Pre-exponential factor |
|---|---|---|
| 1. $CaCO_3 \rightarrow CaO + CO_2$ | 169000 | 1.18 $\times 10^6$ $mol/m^2 s$ |
| 2. $2CaO + SiO_2 \rightarrow C2S$ | 240000 | 9 $\times 10^5$ $m^3/kg\ s$ |
| 3. $C2S + CaO \rightarrow C3S$ | 420000 | 1.3 $\times 10^8$ $m^3/kg\ s$ |
| 4. $3CaO + Al_2O_3 \rightarrow C3A$ | 310000 | 1$\times 10^7$ $m^3/kg\ s$ |
| 5. $4CaO + Al_2O_3 + Fe_2O_3 \rightarrow C4AF$ | 330000 | 1$\times 10^7$ $m^3/kg\ s$ |

*Mujumdar and Ranade (2006a)

## 6. RESULTS AND DISCUSSION

Results obtained by the model are compared with available data of the rotary kiln in Tab. 5. It can be seen that the model predicts the behavior of the industrial kiln reasonably well. Mass fraction values for C3S, C2S, C3A and C4AF obtained with the model fit in the range defined by the lowest and highest values reported for the rotary kiln in study. Mass fraction for remainder CaO predicted by the model exceeds slightly the highest value reported. This can be due to other compounds taking part in the final composition that were not considered in the present model. The error obtained for the predicted temperature of solids at exit is less than 1%.

Tabela 5: **Model predictions and comparison with available data.**

| | | Lowest value | Highest value | Average value | Model prediction |
|---|---|---|---|---|---|
| 1. | Mass fraction of C3S | 0.4634 | 0.5617 | 0.5182 | 0.5141 |
| 2. | Mass fraction of C2S | 0.1843 | 0.2889 | 0.2302 | 0.2219 |
| 3. | Mass fraction of C3A | 0.0490 | 0.0626 | 0.0545 | 0.0582 |
| 4. | Mass fraction of C4AF | 0.1277 | 0.1368 | 0.1323 | 0.1292 |
| 5. | Mass fraction of CaO | 0.0300 | 0.0070 | 0.0150 | 0.0346 |
| 6. | Temperature of solids at exit (K) | - | - | 1673 | 1662 |
| 7. | Mass flow rate at exit (kg/s) | - | - | 23.2 | 25.27 |

Figure 3 shows temperature profile assumed for the gas phase and the measured temperature profile of the steel shell. The abrupt decrease in the shell temperature during the final part of the kiln is due to coating formation. Figure 4 shows the obtained temperature profile of solids, it can be seen that the maximum temperature of the solids its located near the maximum flame temperature position. During the first part of the kiln. According to Coral (2011) the remaining calcination, which is quite endothermic, occurs at higher rates than the other reactions, which added to the poor heat transfer between hot gases and the bed, causes a reduction in the temperature of the solids bed. As the solids move through the kiln, the endothermic nature of reactions 1, 3 and 4 decreases and the exothermic character of reactions 2 and 5 dominates, this added to the heat transfer from the hot gases to the solids bed , causes the increase in the solid bed temperature.

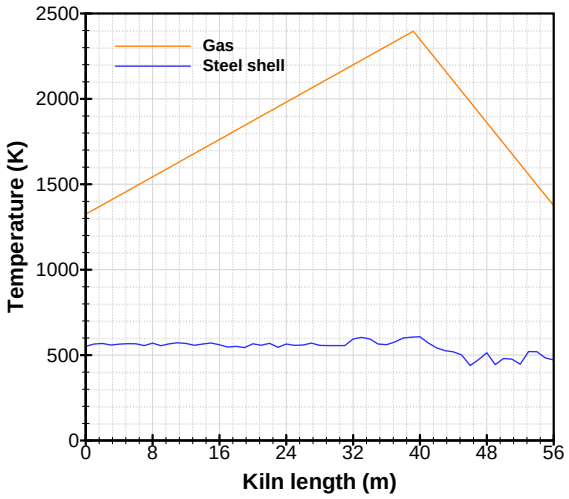


Figura 3: **Temperature profile of gas and shell.** Max. gas temperature: 2396 K at 0.7L.

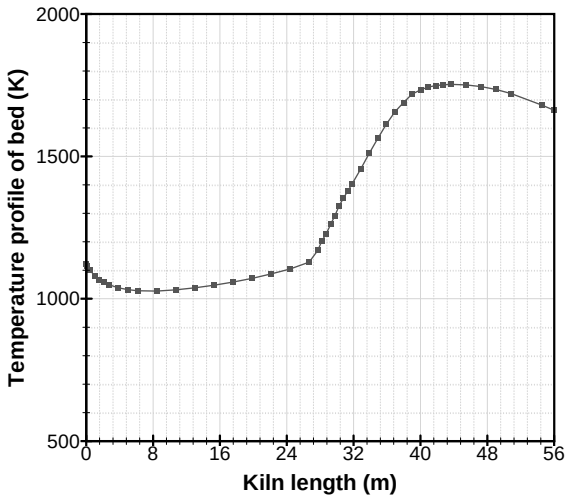


Figura 4: **Temperature profile of solids**

Figure 5 and Figure 6 show the mass fraction profile of the reactives and products along the kiln. In the initial region of the kiln, C2S starts to form as the remaining calcination takes place. This is followed by C3A and C4AF formation. When temperature reaches 1400 K, melting starts to form. Since C3S formation takes place at liquid phase, it starts to form after solids started to melt and this produce a rapid decrease of C2S mass fraction. Figure 7 shows the mass flow rate profile along the kiln. It can be seen that mass flow decreases due to $CO_2$ migration to the gas phase. Once the remaining calcination finishes, the mass flow rate stays constant until kiln exit. The error between the value measured in plant and the value predicted by the mathematical model is around 9%. Coral (2011) explained that discrepancy can be caused by the assumption that the only source of variation of the mass flow is $CO_2$ migration, but this variation can be also caused by solids particle entrainment in the gas region and stagnation of solid material within the kiln.

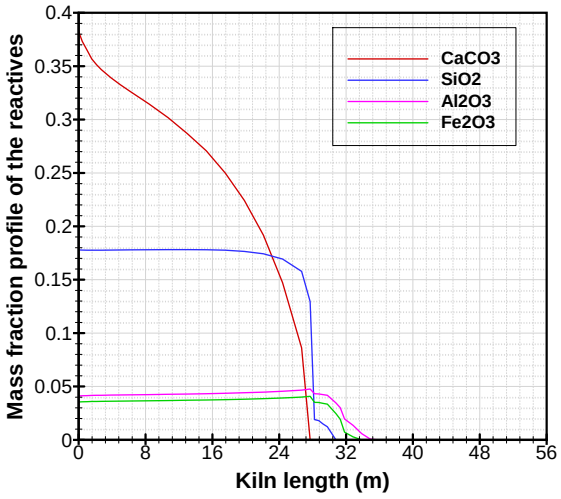


Figura 5: **Mass fraction profile of reactives**

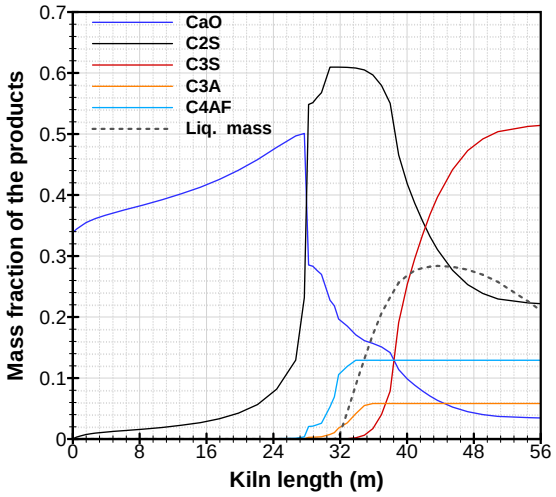


Figura 6: **Mass fraction profile of products**

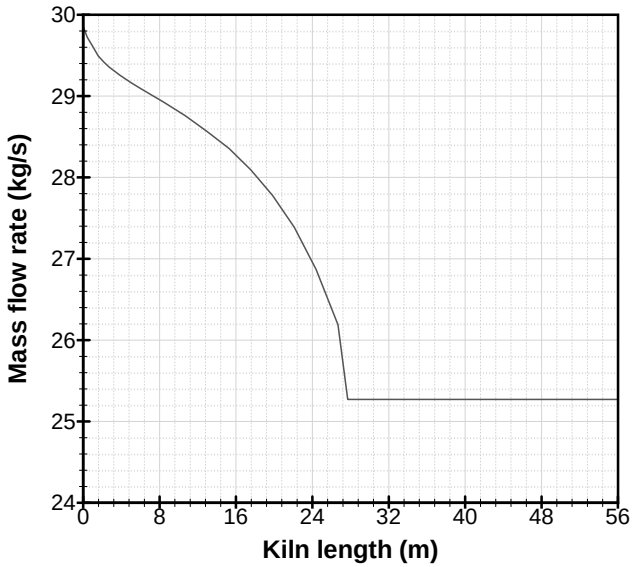


Figura 7: **Mass flow rate along the kiln.**

During simulations, it was found that as the maximum flame temperature increases, the bed temperature and the C3S mass fraction at bed exit also increase as reported by Mujumdar and Ranade (2006a). This is expected since increasing the maximum flame temperature would provide more energy to the bed. It was also understood the influence of the rotational speed in the kiln overall performance. Changes in the rotational speed causes changes in the bed height, therefore in the area exposed to the gas phase. As kiln RPM increases, this area decreases. According to Mujumdar and Ranade (2006a), results indicates that it seems beneficial to operate the kiln at lower revolutions. On the other hand, variation of mass flow rate also affects the kiln performance. Since more mass is flowing, more energy is necessary to get the bed to the temperature where chemical reactions occur, hence, increasing the mass flow rate will also increase the energy consumption of the kiln.

## 7. CONCLUSIONS

An industrial kiln from Paraguay was selected for the one-dimensional model to simulate its performance. Data provided, such temperature of solids and mass fraction of species at solids inlet were used as the initial condition to the model. The external shell temperature profile was obtained by measurable data. Heat transfer in the transverse plane of the solids, variation of the bed height within the kiln, melting and formation of coating were considered in the model. The reactions in solid phase were modeled as a pseudo-homogenous approximation. The calcination reaction was modeled as a shrinking core model reaction, and the pre-exponential factors and activation energy used in the Arrhenius expressions

for the remaining reactions were chosen by trial since they were considered as ad hoc models. For the simulation of the industrial kiln maximum temperature of freeboard gas and its position was set to predict the mass fractions and temperature of bed solids at the exit of the kiln, finding that the obtained results were within usual range. The model was used to understand the influence of operating conditions such rotational speed of kiln and mass flow of solids. Also, it was observed the influence of the position of maximum temperature on the composition and temperature of bed solids at the exit. The results from the model were compared with data, finding the mass fraction within the range and the bed temperature with a maximum difference of 0.7% from data. From the results obtained we concluded that the model presented in this work describes quite well the chemical reactions and thermo-physical phenomenons.

## 8. REFERENCES


, 2005. *Harbison-Walker Handbook of Refractory Practice*. Harbison-Walker Refractories Company, 400 Fairway Drive. Moon Township, PA 15108.

Al-Yasiri, A. and Muhammed, M.A., 2012. "Estimating the thickness of coating in the burning zone of cement kilns including the aging factor". *Iraqi Journal of Mechanical and Material Eng.*, Vol. 12, pp. 459–477.

Boateng, A.A. and Barr, P.V., 1996. "A thermal model for the rotary kiln including heat transfer within the bed". *Int. J. Heat Mass Transfer*, Vol. 39, pp. 2131–2147.

Coral, J.D., 2011. *Diseño de una herramienta computacional para el análisis del desempeño energético de reactores rotatorios para la producción de cemento*. Master's thesis, Universidad Nacional de Colombia.

Danish, M. and Kumar, S., 2012. "Exact analytical solution for the bed depth profile of solids flowing in a rotary kiln". *Powder Technology*, Vol. 230, pp. 29–35.

Darabi, P., 2007. *A mathematical model for cement kiln*. Master's thesis, The University of British Columbia.

Duda, W.H., 1977. *Manual Tecnológico del Cemento*. Editores Tecnicos Asociados S.A., Barcelona, Spain.

Guo, Y., Chan, C. and Lau, K., 2003. "Numerical studies of pulverized coal combustion in a tubular coal combustor with slanted oxygen jet". *Fuel*, Vol. 82, No. 8, pp. 893–907.

Hottel, H.C. and Sarofim, A.F., 1967. *Radiative Transfer*. McGraw-Hill, New York, USA, 1st edition.

Irfan, A. and Doğu, G., 2001. "Calcination kinetics of high purity limestones". *Chemical Engineering Journal*, Vol. 83, No. 2, pp. 131–137.

Lebas, E., Hanrot, F., Ablitzer, D. and Houzelot, J.L., 1995. "Experimental study of residence time, particle movement and bed depth profile in rotary kiln". *Canadian Journal of Chemical Engineering*, Vol. 73, pp. 173–180.

Martin, G., 1932. *Chemical Engineering and Thermodynamics Applied to the Cement Rotary Kiln*. The Technical Press, London, UK.

Mastorakos, E., Massias, A., Tsakiroglou, C.D., Goussis, D.A., Burganos, V.N. and Payatakes, A.C., 1999. "CFD predictions for cement kilns including flame modelling, heat transfer and clinker chemistry". *Applied Mathematical Modelling*, Vol. 23, pp. 55–76.

Mujumdar, K.S., Ganesh, K.V., Kulkarni, S.B. and Ranade, V.V., 2007. "Rotary Cement Kiln Simulator (RoCKS): Integrated modeling of pre-heater, calciner, kiln and clinker cooler". *Chemical Engineering Science*, Vol. 62, pp. 2590–2607.

Mujumdar, K.S. and Ranade, V.V., 2006a. "Simulation of rotary cement kilns using a one-dimensional model". *Chemical Engineering Research and design*, Vol. 84, pp. 165–177.

Mujumdar, K.S. and Ranade, V.V., 2008. "Cfd modeling of rotary cement kilns". *Asia- Pac. J. Chem. Eng.*, Vol. 3, pp. 106–118.

Mujumdar, K.S., Ranade, V.V. and Arora, A., 2006b. "Modeling of rotary cement kilns: Applications to reduction in energy consumption". *Ind. Eng. Chem. Res.*, Vol. 45, pp. 2315–2330.

Ngako, S., Mouangue, R., Caillat, S., Kuitche, A. and Saragba, E., 2015. "Numerical investigation of bed depth height, axial velocity and mean residence time of inert particles in steady state industrial cement rotary kiln: Case of Figuil Plant in Cameroon". *Powder Technology*, Vol. 271, pp. 221–227.

Perry, R.H., 1997. *Perry's Chemical Engineers' Handbook*. McGraw-Hill, New York, USA, 7th edition.

Rao, T.R. and Bowen, J.H., 1989. "Kinetics of calcium carbonate decomposition". *Chem. Eng. Res. Des.*, Vol. 67, pp. 38–47.

Saeman, W.C., 1951. "Passage of solids through rotary kilns: factors affecting time of passage". *Chemical Engineering Process*, Vol. 47, pp. 508–514.

Silcox, G.D. and Perching, D.W., 1990. "The effects of rotary kiln operating conditions and design on burden heating rates as determined by a mathematical model of rotary kiln heat transfer". *Journal of the Air & Waste Management Association*, Vol. 40, No. 3, pp. 337–344.

Spang, H., 1972. "A dynamic model of a cement kiln". *Automatica*, Vol. 8, No. 3, pp. 309–323.

Taylor, H.F., 1990. *Cement Chemistry*. Academic Press Inc., San Diego, USA.

Tscheng, S.H. and Watkinson, A.P., 1979. "Convective transfer in rotary kilns". *Can. J. Chem. Eng.*, Vol. 57, pp. 433–443.


## 9. RESPONSIBILITY NOTICE

The authors are the only responsible for the printed material included in this paper.